THE JOURNAL OF BIOLOGICAL CHEMISTRY
Vol. 278, No. 33, Issue of August 15, pp. 31095–31104, 2003
Printed in U.S.A.

A Maurotoxin with Constrained Standard Disulfide Bridging

INNOVATIVE STRATEGY OF CHEMICAL SYNTHESIS, PHARMACOLOGY, AND DOCKING ON K^+ CHANNELS*

Received for publication, April 23, 2003, and in revised form, May 26, 2003
Published, JBC Papers in Press, June 3, 2003, DOI 10.1074/jbc.M304271200

Sarrah M'Barek,[a] Ignacio Lopez-Gonzalez,[b,c] Nicolas Andreotti,[a] Eric di Luccio,[a] Violeta Visan,[d] Stephan Grissmer,[d] Susan Judge,[e] Mohamed El Ayeb,[f] Hervé Darbon,[g] Hervé Rochat,[a] François Sampieri,[a] Evelyne Béraud,[h] Ziad Fajloun,[a] Michel De Waard,[b] and Jean-Marc Sabatier[a,i]

From the [a]Laboratoire International Associé d'Ingénierie Biomoléculaire, CNRS Unité Mixte de Recherche 6560 Bd Pierre Dramard, 13916 Marseille Cedex 20, France, [b]Inserm EMI 9931, Commissariat à l'Energie Atomique, Institut Fédératif de Recherche 27, Département de Recherche Dynamique Cellulaire, Canaux Ioniques et Signalization, 17 rue des Martyrs, 38054 Grenoble Cedex 09, France, [d]Universität Ulm, Albert Einstein-Allee 11, D-89081 Ulm, Germany, the [e]University of Maryland School of Medicine, Baltimore, Maryland 21201-1509, the [f]Laboratoire des Venins et Toxines, Institut Pasteur de Tunis, P. O. Box 74, 1002 Belvédère, Tunis, Tunisia, [g]Architecture et Fonction des Macromolécules Biologiques, CNRS Unité Propre de Recherche 9039, 31 Chemin Joseph Aiguier, 13402 Marseille, France, and the [h]Laboratoire d'Immunologie, Faculté de Médecine Timone, 27 Bd Jean Moulin, 13385 Marseille Cedex 5, France

Maurotoxin (MTX) is a 34-residue toxin that has been isolated initially from the venom of the scorpion *Scorpio maurus palmatus*. It presents a large number of pharmacological targets, including small conductance Ca^{2+}-activated and voltage-gated K^+ channels. Contrary to other toxins of the α-KTx6 family (Pi1, Pi4, Pi7, and HsTx1), MTX exhibits a unique disulfide bridge organization of the type C1-C5, C2-C6, C3-C4, and C7-C8 (instead of the conventional C1-C5, C2-C6, C3-C7, and C4-C8, herein referred to as Pi1-like) that does not prevent its folding along the classic α/β scaffold of scorpion toxins. Here, we developed an innovative strategy of chemical peptide synthesis to produce an MTX variant (MTX_{Pi1}) with a conventional pattern of disulfide bridging without any alteration of the toxin chemical structure. This strategy was used solely to address the impact of half-cystine pairings on MTX structural properties and pharmacology. The data indicate that MTX_{Pi1} displays some marked changes in affinities toward the target K^+ channels. Computed docking analyses using molecular models of both MTX_{Pi1} and the various voltage-gated K^+ channel subtypes (*Shaker* B, $K_v1.2$, and $K_v1.3$) were found to correlate with MTX_{Pi1} pharmacology. A functional map detailing the interaction between MTX_{Pi1} and *Shaker* B channel was generated in line with docking experiments.

Maurotoxin (MTX)[1] is a basic 34-residue toxin that has been initially isolated from the venom of the Tunisian chactidae scorpion *Scorpio maurus palmatus* (1, 2). Together with Pi1 (3), Pi4 (4), Pi7 (4), and HsTx1 (5, 6), MTX belongs to a family of short-chain scorpion toxins (α-KTx6) cross-linked by four disulfide bridges (7). MTX has many pharmacological targets: it binds onto apamin-sensitive small conductance Ca^{2+}-activated K^+ (SK) channels (1, 2, 8) and potently acts on intermediate-conductance Ca^{2+}-activated K^+ (IK) channels (8) as well as several subtypes of voltage-gated K_v channels (*Shaker* B, Kv1.2, and Kv1.3) (1, 2, 8–10). The three-dimensional structure of MTX in solution (11) consists of a bent α-helix (residues 6–17) connected by a loop to a two-stranded antiparallel β-sheet (residues 22–25 and 28–31). Such a structural motif is termed the α/β scaffold (12), which occurs independently of scorpion toxin chain length and ion channel selectivity, except for Ca^{2+} channel-acting toxins (13). The α/β scaffold is associated with the presence of a consensus sequence of the type [. . .]C[. . .]C*XXXX*C[. . .](G/A/S)*X*C[. . .]C*X*C[. . .] (12), or its variants such as [. . .]C[. . .]C*XX*PC[. . .]C[. . .](G/A/S)*X*C[. . .] C*X*C[. . .] in the cases of MTX, Pi1, Pi4, Pi7, and HsTx1 (2, 6, 11, 14, 15). It is worth noting that the integrity of the α/β scaffold is maintained by the connection of the α-helix to the antiparallel β-sheet by two of the three or four disulfide bridges, depending on the scorpion toxin considered. The pharmacological profile of a particular toxin can be inferred to the spatial positioning of key amino acid residues required for ion channel recognition. The spatial positioning of those crucial residues depends on the toxin primary structure and the associated specific arrangement of half-cystine pairs (16–18). In the case of MTX, the disulfide bridging is normally of the uncommon C1-C5, C2-C6, C3-C4, and C7-C8 type (Fig. 1*A*). However, MTX is able to adopt the standard C1-C5, C2-C6, C3-C7, and C4-C8 arrangement (as observed in other α-KTx6 members) consecutive to selective amino acid residue substitution(s) (16–18). The latter concerned Lys^{15}, Gly^{33} (18), or Pro^{12} and Pro^{20} (17) of MTX and were found to markedly affect peptide affinities toward the various K^+ channel subtypes. Though the substituted residues were mainly selected on the basis of a pre-

* This work was supported by CNRS, INSERM, the Commissariat à l'Energie Atomique, and Cellpep S.A. The costs of publication of this article were defrayed in part by the payment of page charges. This article must therefore be hereby marked "*advertisement*" in accordance with 18 U.S.C. Section 1734 solely to indicate this fact.

[c] A fellowship recipient from the French Ministry of Research and Technology.
[i] To whom correspondence should be addressed. Tel.: 33-4-91-69-88-52; Fax: 33-4-91-65-75-95; E-mail: sabatier.jm@jean-roche.univ-mrs.fr.

[1] The abbreviations used are: MTX, synthetic maurotoxin (toxin from the scorpion *S. maurus palmatus*); MTX_{Pi1}, synthetic maurotoxin with imposed standard (Pi1-like) disulfide bridging; MTX_{Tyr}, reduced or oxidized form of synthetic maurotoxin with a 2,6 dichloro-benzyl protecting group on the side-chain phenol ring of Tyr in position 32; HsTx1, toxin 1 from the scorpion *Heterometrus spinnifer*; Pi1, Pi4, Pi7, toxins 1, 4, and 7, from the scorpion *Pandinus imperator*; HPLC, high pressure liquid chromatography; Fmoc, N^a-(9-fluorenyl)methyloxycarbonyl; SK and IK channels, small- and intermediate-conductance Ca^{2+}-activated K^+ channels, respectively; K_v channels, mammalian voltage-gated K^+ channels; KvAP, a voltage-dependent K^+ channel from *A. pernix*; *Shaker* B channel, insect voltage-gated K^+ channels; TFMSA, trifluoromethanesulfonic acid.

sumptive non-implication regarding ion channel recognition, one cannot rule out that they not only affect half-cystine pairings but also the spatial distribution of key toxin amino acid residues.

In the present work, we examined for the first time the sole contribution of the disulfide bridge arrangement on toxin pharmacology by maintaining unchanged the MTX primary structure. The aim was to produce and characterize an MTX variant adopting conventional Pi1-like disulfide bridges, referred to as MTX_{Pi1} (Fig. 1*A*). For this purpose, we developed an innovative strategy of solid-phase peptide synthesis based on a temporary chemical modification of the side chain of a trifunctional MTX amino acid residue (Tyr^{32}) expected to guide the type of toxin half-cystine pairings (Fig. 1*B*). We focused on the Tyr^{32} residue because formation of the short Cys^{31}-Cys^{34} (C7-C8) disulfide bridge (referred to as a 14-member disulfide ring) is very sensitive to local steric hindrance. Indeed, we have previously shown that replacement of the side-chain hydrogen atom of Gly^{33} by a larger methyl group of Ala prevents the C7-C8 connection and forces the corresponding synthetic MTX analogue ([Ala^{33}]-MTX) to adopt the conventional Pi1-like disulfide bridge arrangement of other α-KTx6 members (18). This novel pattern of half-cystine pairings (C1-C5, C2-C6, C3-C7, and C4-C8) comprises the reorganization of two of the four disulfide bridges (C3-C7 and C4-C8, *versus* C3-C4 and C7-C8). The following approach was experimentally developed to produce MTX_{Pi1} (Fig. 1*B*). (i) A classic stepwise solid-phase assembly of MTX peptide chain using a combination of Fmoc chemistry and *t*-butyl-type side-chain protecting groups for trifunctional amino acid residues (19). In the case of Tyr^{32}, a more acid-resistant 2,6 dichloro-benzyl group was used to protect its phenol ring. (ii) A trifluoroacetic acid treatment to remove all *t*-butyl-type protecting groups and to cleave the peptide from the resin. (iii) An oxidative folding of the Tyr^{32}-protected MTX (MTX_{Tyr}), and (iv) a final trifluoromethanesulfonic acid (TFMSA) treatment of the folded/oxidized MTX_{Tyr} to remove the Tyr^{32} side-chain protecting group, thereby generating MTX_{Pi1} (20). Using this procedure, we succeeded in the chemical production of MTX_{Pi1} and demonstrate that its novel, but conventional, disulfide bridging is accompanied by marked differences in toxin properties.

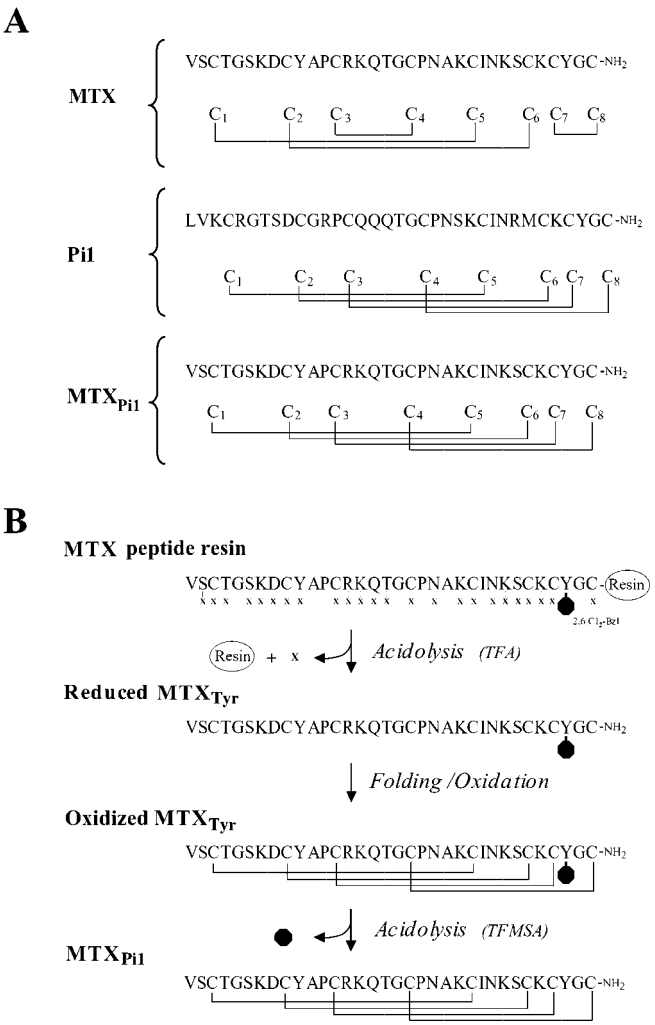

FIG. 1. **Half-cystine pairings of MTX, Pi1, and MTX_{Pi1} and strategy for the chemical synthesis of MTX_{Pi1}.** *A*, primary structures and corresponding half-cystine pairings of MTX, Pi1, and MTX_{Pi1}. *B*, strategy used for the chemical synthesis of MTX_{Pi1}. The phenol ring of Tyr^{32} from reduced MTX remains protected with the 2,6 dichloro-benzyl group after trifluoroacetic acid treatment (reduced MTX_{Tyr}) of the MTX peptide resin, whereas the side-chain protecting groups (*t*-butyl-type denoted *X*) of other trifunctional amino acid residues are removed. The reduced MTX_{Tyr} folds/oxidizes to yield the oxidized MTX_{Tyr} with Pi1-like half-cystine pairings. Removal of the 2,6 dichloro-benzyl group by TFMSA treatment of the folded/oxidized MTX_{Tyr} generates MTX_{Pi1}.

EXPERIMENTAL PROCEDURES

Materials

N-α-Fmoc-L-amino acids, Fmoc-amide resin, and reagents used for peptide synthesis were obtained from PerkinElmer, except *N*-α-Fmoc-L-Tyr(2,6 dichloro-benzyl)-OH, which was from Fluka. Solvents were analytical-grade products and purchased from SDS. Enzymes (trypsin and chymotrypsin) were obtained from Roche Applied Science.

Chemical Synthesis and Characterization of MTX_{Pi1}

The MTX_{Pi1} variant was assembled by the solid-phase technique (19) using a peptide synthesizer (Model 433A; Applied Biosystems Inc.). Peptide chains were assembled stepwise on 0.35 milliequivalent of Fmoc-amide resin (0.66 milliequivalent of amino group/g) using 1 mM Fmoc amino acid derivatives. The side-chain protecting groups used for trifunctional residues were: trityl for Cys, Asn, and Gln; *t*-butyl for Ser, Tyr, Thr, and Asp; pentamethylchroman for Arg; *t*-butyloxycarbonyl for Lys; and 2,6 dichloro-benzyl for Tyr in position 32. The Fmoc-amino acid derivatives were coupled (20 min) as their hydroxybenzotriazole active esters in *N*-methylpyrrolidone (2.8-fold excess). The fully protected peptide resin (2.5 g) was treated for 2.5 h at 25 °C with a mixture of trifluoroacetic acid/H_2O/thioanisole/ethanedithiol (73:11:11:5, v/v) in the presence of crystalline phenol (2.5 g). Under this condition, the peptide is cleaved from the resin and all its side-chain protecting groups are removed, except the 2,6 dichloro-benzyl protecting group of Tyr^{32}. After filtration of the mixture, the crude Tyr^{32}-protected peptide (MTX_{Tyr}) was precipitated and washed by adding cold diethyloxide. The crude MTX_{Tyr} was pelleted by centrifugation (3,000 $\times$ *g*; 10 min), and the supernatant was discarded. The reduced MTX_{Tyr} was then dissolved at 2 mM concentration in 0.2 M Tris-HCl buffer, pH 8.3, and stirred under air to allow oxidative folding (72 h, 25 °C). The folded/oxidized MTX_{Tyr} peptide was purified by reversed-phase high-pressure liquid chromatography (HPLC) (PerkinElmer, C_{18} Aquapore ODS 20 μM, 250 $\times$ 10 mm) by means of a 60-min linear gradient of 0.08% (v/v) trifluoroacetic acid/0% to 35% acetonitrile in 0.1% (v/v) trifluoroacetic acid/H_2O at a flow rate of 5 ml/min (λ = 230 nm). The purified oxidized MTX_{Tyr} (10 mg) was treated for 10 min at 25 °C with a 10.25-ml mixture of trifluoroacetic acid/H_2O (97.5:2.5, v/v) in the presence of crystalline phenol (1.5 g) and *p*-cresol (1 g). Next, the mixture was chilled on ice before addition of 1 ml of neat trifluoromethanesulfonic acid (20). The new mixture was then incubated for an additional 20 min to remove the 2,6 dichloro-benzyl protecting groups from oxidized MTX_{Tyr}, thereby yielding MTX_{Pi1}. The peptide was then filtrated, precipitated, and washed as described for MTX_{Tyr} after the first trifluoroacetic acid cleavage. The homogeneity and identity of MTX_{Pi1} was assessed by: (i) analytical C_{18} reversed-phase HPLC, (ii) amino acid analysis after acidolysis, (iii) Edman sequencing, (iv) mass determination by matrix-assisted laser desorption ionization-time of flight mass spectrometry, and (v) enzyme-based cleavage for half-cystine pairing determination.

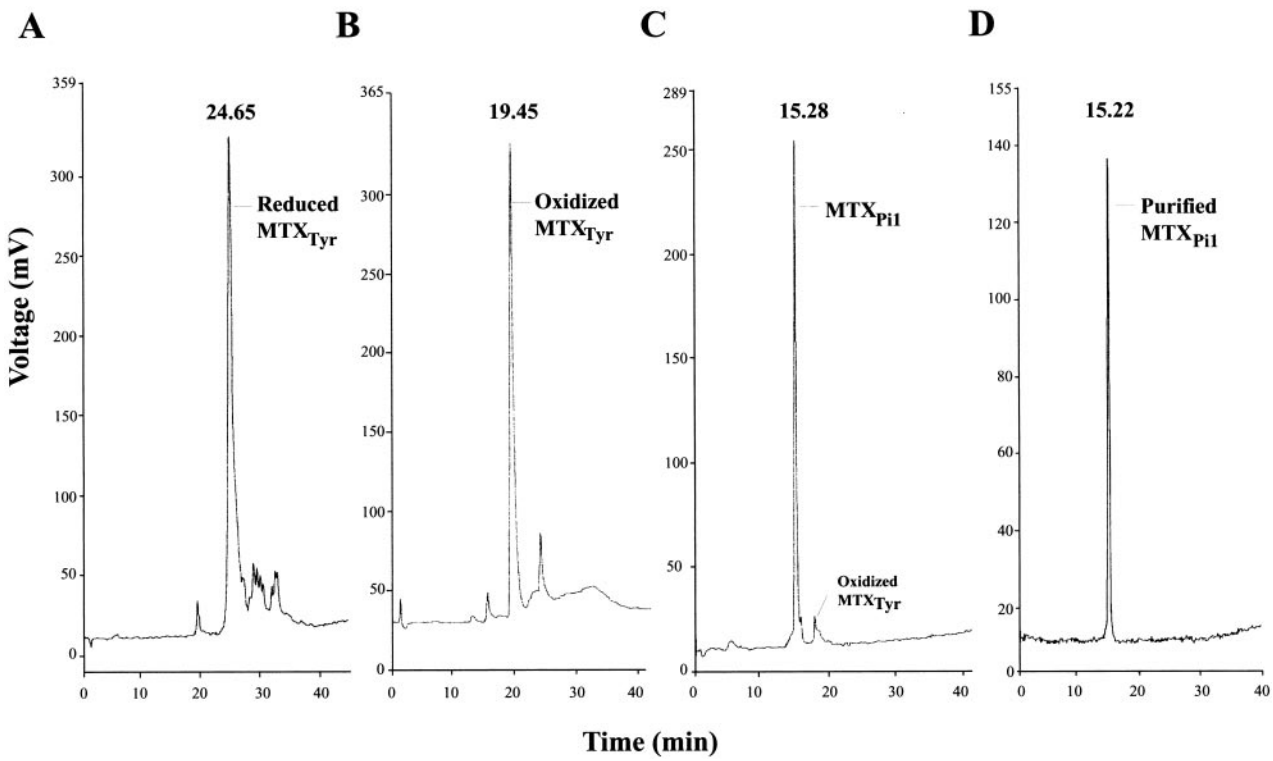

FIG. 2. **Chemical synthesis of MTX_{Pi1}.** *A*, analytical C_{18} reversed-phase HPLC elution profile of crude reduced MTX_{Tyr} after trifluoroacetic acid treatment. *B*, crude folded/oxidized MTX_{Tyr} after oxidative folding. *C*, MTX_{Pi1} after TFMSA treatment of folded/oxidized MTX_{Tyr}. *D*, purified MTX_{Pi1}.

Assignment of Half-cystine Pairings of MTX_{Pi1} by Enzyme-based Cleavage and Edman Sequencing Analysis

MTX_{Pi1} (800 μg) was incubated with a mixture of trypsin and chymotrypsin at 10% (w/w) in 0.2 M Tris-HCl, pH 7.4, for 12 h at 37 °C. The resulting peptide fragments were then purified by reversed-phase HPLC (Chromolith RP18, 5 μM, 4.6 × 100 mm) with a 60-min linear gradient of 0.08% (v/v) trifluoroacetic acid /0–60% acetonitrile in 0.1% (v/v) trifluoroacetic acid/H_2O at a flow rate of 1 ml/min (λ = 230 nm) and freeze-dried prior to their analyses. These peptide fragments were hydrolyzed by acidolysis (6 N HCl/phenol), b and their amino acid contents were determined (System 6300 amino acid analyzer; Beckman). The fragments were further characterized by mass spectrometry analysis (RP-DE Voyager; Perseptive Biosystems) and Edman sequencing using a gas-phase microsequencer (Applied Biosystems 470A). In standard HPLC conditions for analyzing phenylthiohydantoin (PTH) amino acid derivatives, diPTH-cystine elutes at a retention time of 9.8 min.

Circular Dichroism Analyses of MTX_{Pi1}, MTX, and Pi1

Circular dichroism (CD) spectra were obtained on a Jasco J-810 spectropolarimeter equipped with a PTC-423S thermostat. A ratio of 2:20 was found between the positive CD band at 290.5 nm and the negative band at 192.5 nm. CD spectra were reported as the absorption coefficient ($\Delta\epsilon$) per amide. The far UV CD spectra were acquired at 20 °C in H_2O between 185 and 260 nm using a 0.1-cm path length cell. Data were collected twice at 0.6-nm intervals with a scan rate of 50 nm/min. As assessed by amino acid analysis, the concentration of MTX_{Pi1}, MTX, or Pi1 was 40 nM.

Toxin Docking on Voltage-gated K^+ Channels

Atomic Coordinates—Atomic coordinates of MTX was obtained from the Swiss Protein Data base (Swiss-Prot www.expasy.ch) (number 1TXM).

Molecular Modeling—Molecular modeling of the S5-H5-S6 portions of rat $K_v1.1$, $K_v1.2$, $K_v1.3$, and *Drosophila Shaker* B channels was achieved on the basis of the crystal structure of the KcsA channel solved at a resolution of 3.2 Å (Swiss-Prot number 1BL8). The three-dimensional structural models of these channels were generated by using KcsA as a template and with the biopolymer homology modeling software of Swiss-model/Deep view 3.7 (Swiss-Prot, Switzerland). Amino acid sequence alignments between KcsA and $K_v1.1$, $K_v1.2$, $K_v1.3$, or *Shaker* B channels, which were generated by using CLUSTALW (V.1.82, www.ebi.ac.uk/clustalw/), showed that homologies are 69.8, 70.1, 69.1, and 65.6%, respectively. To avoid steric overlaps and clashes, modeled side chains and Cα backbones of K^+ channels were subjected to energy refinement (until $\Delta\epsilon E < 0.05$ kJ·mol^{-1}·Å^{-1}) using, successively, steepest-descent, conjugate gradient, and Newton Raphson algorithms, with the consistent valence force-field as implemented in the INSIGHT II Discover3 module (1998 release, Molecular Simulations Inc., ACCELRYS, San Diego, CA). Root mean square deviation values between the KcsA template Cα backbone and the modeled $K_v1.1$, $K_v1.2$, $K_v1.3$, and *Shaker* B Cα backbones were 0.48, 1.93, 0.32, and 1.68 Å, respectively.

A molecular model of Pi1 was obtained on the basis of the three-dimensional structure of MTX in solution (Swiss-Prot number 1TXM) by using the homology method of Swiss-Model/Deep view 3.7. Disulfide bridges were assigned using the Biopolymer module of InsightII. Similarly, this module was used to generate the molecular model of MTX_{Pi1}. Molecular models were relaxed by 5,000 steps of 1 fs of dynamics simulation at 15 K, then minimized by energy refinement (until $\Delta\epsilon E <$ 0.05 kJ·mol^{-1}·Å^{-1}) using the algorithms and force field previously described for $K_v1.1$, $K_v1.2$, $K_v1.3$, and *Shaker* B channels. Amino acid sequence alignment between Pi1 and MTX (CLUSTALW) points to 88.2% sequence homology. Root mean square deviation values between template MTX Cα backbone and the modeled Pi1 and MTX_{Pi1} Cα backbones were 1.33 and 1.05 Å, respectively. Geometric quality of all models was evaluated using PROCHECK V3.5.4 (21, 22).

Protein Docking—Molecular interaction simulations were performed using the BiGGER program (bimolecular complex generation with global evaluation and ranking) (23). In the first step, a 1-Å three-dimensional matrix composed of small cubic cells, which represents the complex shape of each molecule, was generated. The translational interaction space was searched for each relative orientation of the two molecules by systematically shifting the probe matrix (toxin) to the target matrix (ion channel). 5,000 docking solutions were selected after probe rotation of 15° relative to the target, and this surface matching was repeated until a complete non-redundant search was achieved. The algorithm used by BiGGER performs a complete and systematic search for surface complementarities (both geometry complementarities and amino acid residue pairwise affinities are considered) between two potentially interacting molecules and enables an implicit treatment of molecular flexibility. In the second step, the 5,000 putative solutions

A

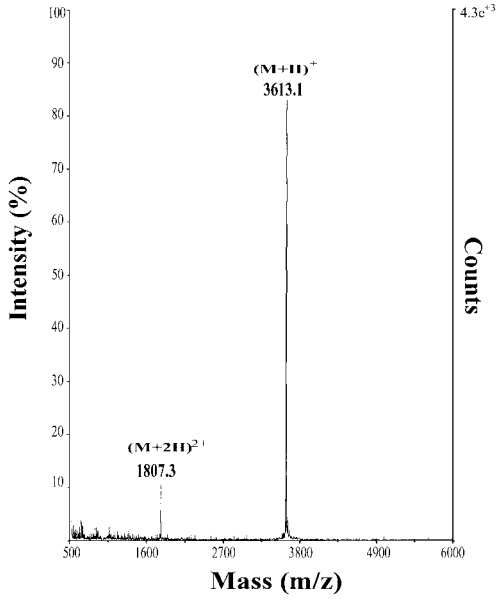

B

MTX_{Pi1}	
Deduced M_r(M+H)$^+$	3613.3
Experimental M_r(M+H)$^+$	3613.1
Amino acid analysis	
Asx	2.9 (3)
Thr	1.9 (2)
Ser	2.7 (3)
Glx	1.0 (1)
Gly	3.0 (3)
Ala	2.0 (2)
Val	1.0 (1)
Cys	7.8 (8)
Ile	0.9 (1)
Tyr	1.9 (2)
Lys	5.0 (5)
Arg	0.9 (1)
Pro	1.9 (2)

C

Enzymes	Retention Time (min)	Proteolytic Fragments	Experimental M_r (M+H)$^+$	Deduced M (M+H)$^+$	Half-Cystine Pairings
Trypsin + Chymotrypsin	2.1	^{9}DCY SCK^{29}	734.0	734.8	Cys^{9}-Cys^{29}
	17.4	^{3}VSCTGCSK CINK^{24}	1156.2	1156.4	Cys^{3}-Cys^{24}
	18.5	^{13}APCR CY^{31}	727.2	726.9	Cys^{13}-Cys^{31}
	21.8	^{19}TGCPNAK GC^{34}-NH_2	868.5	868.0	Cys^{19}-Cys^{34}

D

FIG. 3. **Physicochemical characterization and disulfide bridge organization of MTX_{Pi1}.** *A*, mass spectrum (matrix-assisted laser desorption/ionization-time of flight) of MTX_{Pi1}. *B*, amino acid analysis of purified MTX_{Pi1} after acidolytic cleavage. *C*, assignment of the half-cystine pairings by analysis of the peptide fragments yielded by enzyme cleavage (trypsin and chymotrypsin) of MTX_{Pi1}. *D*, primary structure and Pi1-like disulfide bridge pattern of MTX_{Pi1}.

were ranked according to four different interaction terms: surface matching, side-chain contacts, electrostatic, and solvation energies combined into a global scoring function.

Docking Solution Screening—The 15 best solutions were selected according to (i) the global score from BiGGER, (ii) toxin Lys residue (Lys^{23} for MTX and MTX_{Pi1}, or Lys^{24} for Pi1) and β-sheet strand orientations toward the ion channel pore, and (iii) the best orientation, considering the electrostatic properties of both the toxin and the K^+ channel. The GRASP software (24) was used to determine these electrostatic properties (GRASP; Howard Hughes Medical Institute, Columbia University, New York).

Structural Refinement of the Final Complexes—The screened docking solutions were minimized with a rigid-body method (Cα-locked) with steepest-descent algorithms using Deep-view V3.7 (until $\Delta\epsilon E < 0.05$ kJ·mol^{-1}·Å^{-1}) with a GROMOS96 force field (25) to relieve possible steric clashes and overlaps. During structural refinement, a distance-dependent dielectric constant of 4 was used.

Docking Energy Calculations—Final docking energy of each best solution ($\epsilon_{toxin-channel} - \epsilon_{toxin} + \epsilon_{channel}$)) was obtained by subtracting the sum of toxin energy alone (ϵ_{toxin}) and ion channel energy alone ($\epsilon_{channel}$), after rigid body minimization (Cα−Cα distances locked) until $\Delta\epsilon E < 0.05$ kJ·mol^{-1}·Å^{-1} (GROMOS96 force field) (25), from the final complex energy ($\epsilon_{toxin-channel}$) minimized under identical conditions.

Close Interaction Analyses—Details of interactions were analyzed using the LIGPLOT program (26) on each best docking solution given by the screening method.

Linear Regression—Linear regression was computed using the Prism software (GraphPad Prism version 3.0cx for MacOS X; GraphPad Software, San Diego, CA; www.graphpad.com).

Neurotoxicity of MTX_{Pi1} and MTX_{Tyr} in Mice

The peptides were tested *in vivo* for toxicity by determining the LD_{50} after intracerebroventricular injections into 20 g of C57/BL6 mice (animal testing agreement number 006573, delivered by the Ministère de l'Agriculture et de la Pêche). Groups of six mice per dose were injected with 5 μl of MTX_{Pi1} solution containing 0.1% (w/v) bovine serum albumin and 0.9% (w/v) sodium chloride.

Competitive Inhibition of ^{125}I-Apamin Binding onto Rat Brain Synaptosomes by MTX_{Pi1}, MTX_{Tyr}, and MTX

Rat brain synaptosomes were prepared as described by Gray and Whittaker (27). Aliquots of 50 μl of 0.1 nM ^{125}I-apamin were added to 400 μl of synaptosome suspension (0.4 mg protein/ml). Samples were incubated for 1 h at 4 °C with 50 μl of one of a series of concentrations of MTX_{Pi1} or MTX_{Tyr} or MTX (10^{-2} M to 10^{-14} M) in 500 μl of final

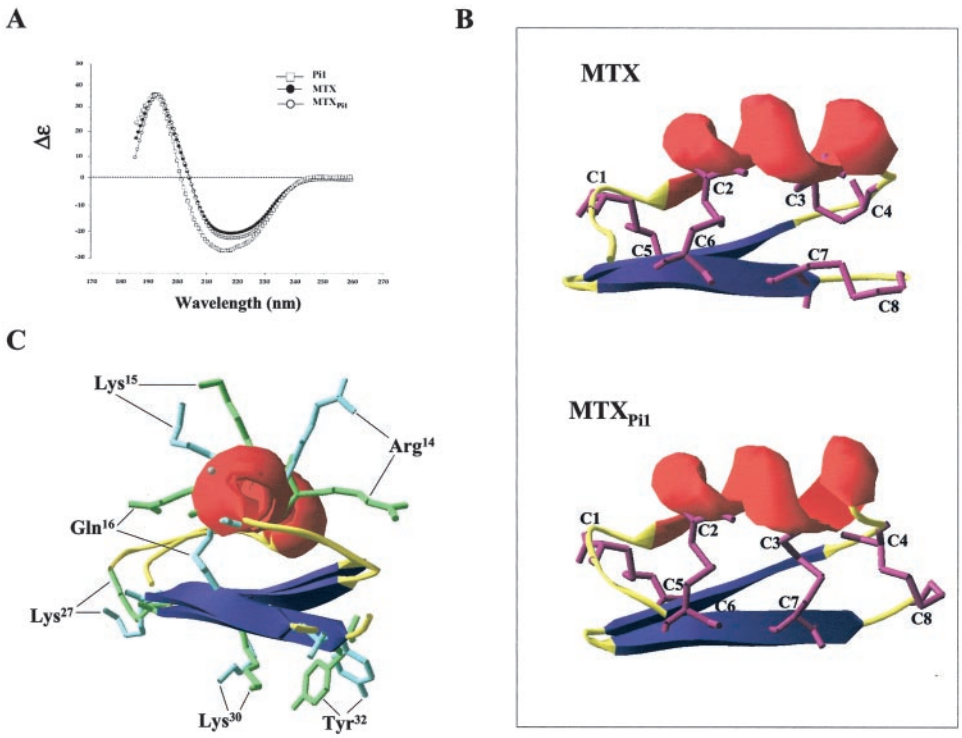

FIG. 4. **Structural analyses of MTX_{Pi1}.** *A*, superimposed CD spectra of MTX_{Pi1}, MTX, and Pi1. *B*, structural comparison of MTX and MTX_{Pi1} Cα backbones. *Top*, MTX with C1-C5, C2-C6, C3-C4, and C7-C8 half-cystine pairings. *Bottom*, MTX_{Pi1} with C1-C5, C2-C6, C3-C7, and C4-C8 pairings. Both peptides are shown as ribbon structures (α-helices, β-sheets, Cα backbones, and disulfide bridges are highlighted in *red*, *blue*, *yellow*, and *purple*, respectively). The three-dimensional structure of MTX in solution (11) is retrieved from the Swiss Protein Data Bank (Swiss-Prot number 1TXM), whereas a molecular model of MTX_{Pi1} was used. The drawing was generated using the Swiss PDB viewer. *C*, superimposed Cα backbones of MTX and MTX_{Pi1}. Side chains, from amino acid residues that are the most differently oriented between both peptides, are detailed in *green* (MTX_{Pi1}) and *blue* (MTX). Disulfide bridges are omitted for clarity.

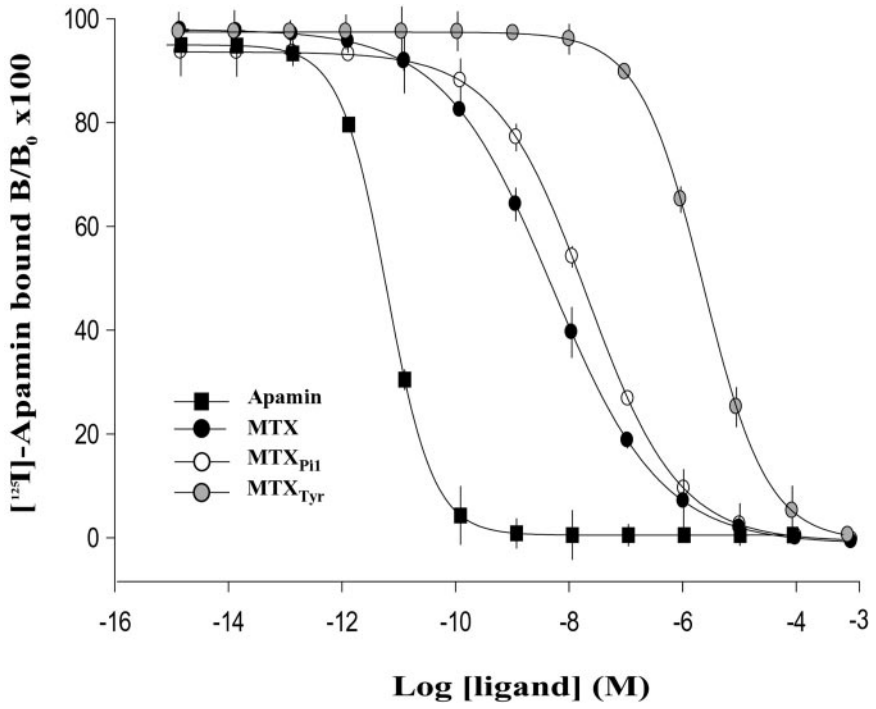

FIG. 5. **Effect of MTX_{Pi1} on the binding of ^{125}I-apamin onto rat brain synaptosomes: Comparison between MTX and MTX_{Tyr}.** B_o is the binding of 0.1 nM ^{125}I-apamin in the absence of ligand, and *B* is the binding in the presence of the indicated concentrations of competitors. Nonspecific binding, less than 8%, was subtracted for the calculation of the ratios. The data were fitted by the equation y = a/[1 + exp(-(x-IC_{50})/b] with IC_{50} values of 4.8 ± 3.8 pM (apamin, *filled squares*), 4.4 ± 3.1 nM (MTX, *filled circles*), 17.4 ± 5.6 nM (MTX_{Pi1}, *open circles*), and 2.6 ± 0.3 μM (MTX_{Tyr}, *gray circles*). Data are the mean of triplicates ± S.D.

volume. The incubation buffer was 25 mM Tris-HCl, 10 mM KCl, pH 7.2. The samples were centrifuged, and the resulting pellets were washed three times in 1 ml of the same buffer. Bound radioactivity was determined by γ counting (Packard Crystal II). The values expressed are the means of triplicate experiments ± S.D. Nonspecific binding, less than 8% of the total binding, was determined in the presence of an excess (10 nM) of unlabeled apamin.

Preparation and Electrophysiological Recordings of Xenopus Oocytes

Xenopus laevis oocytes at stages V and VI were prepared for cRNA injection and electrophysiological recordings. The follicular cell layer was removed by enzymatic treatment with 2 mg/ml collagenase IA (Sigma) in classic Barth's medium lacking external Ca^{2+}. The cDNA

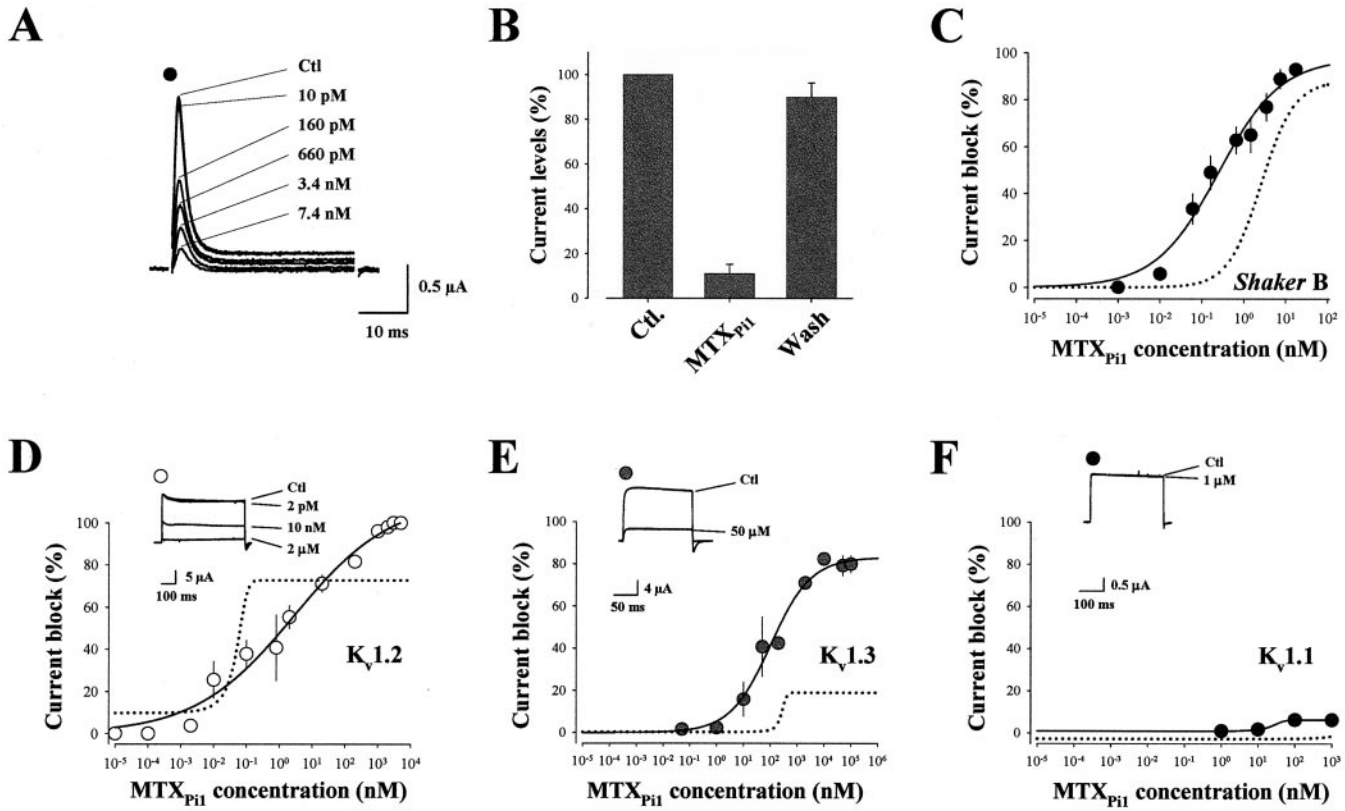

FIG. 6. **MTX_{Pi1} exhibits pharmacological properties distinct from those of MTX.** *A*, MTX_{Pi1} is a high affinity blocker of *Shaker* B channel. Current traces illustrating the extent of current block by various concentrations of MTX_{Pi1}. Holding potential is −80 mV, and test potential is +60 mV. *B*, recovery of *Shaker* B K^+ current after application of 10 nM MTX_{Pi1}. *C*, dose-dependent inhibition curve of *Shaker* B currents by MTX_{Pi1}. Each data point is the mean ± S.D. of $n = 7$ cells. The *solid line* through the data is from the Hill equation $y = y_o + (a.x^b/IC_{50}{}^b + x^b)$ with an IC_{50} value of 0.24 ± 0.12 nM ($n = 63$). a is the maximum block by MTX_{Pi1}, a = 97.7 ± 9.4%. For comparison, the *dotted line* represents the dose-dependent inhibition curve by MTX. *D*, dose-dependent inhibition curve of $K_v1.2$ currents by MTX_{Pi1}. $IC_{50} = 2.76 \pm 2.01$ nM ($n = 84$), and a = 111.6 ± 8.2%. *Dotted line*, the effect of MTX. *E*, dose-dependent inhibition curve of $K_v1.3$ currents by MTX_{Pi1}. $IC_{50} = 102.4 \pm 37.3$ nM ($n = 63$), and a = 83.2 ± 4.2%. *Dotted line*, the effect of MTX. *F*, dose-dependent inhibition curve of $K_v1.1$ currents by MTX_{Pi1}. $IC_{50} = 16.0 \pm 15.9$ nM ($n = 28$), and a = 6.4 ± 1.0%. *Dotted line*, the effect of MTX.

plasmids were linearized with *Sma*I (*Shaker* B), *Not*I (rat $K_v1.1$), *Xba*I (rat $K_v1.2$), and *Eco*R1 (rat $K_v1.3$) and transcribed with either T7 or SP6 RNA polymerase (mMessage mMachine kit; Ambion). The cells were microinjected 1–2 days later with 50 nl of cRNA (0.1 µg/µl *Shaker* B, rat $K_v1.1$, rat $K_v1.2$, or rat $K_v1.3$ channels). To favor K^+ channel expression, cells were incubated at 16 °C into a defined nutrient oocyte medium (28) 2–6 days before current recordings. Oocyte currents were then recorded at 20 °C by standard two-microelectrode techniques using a voltage-clamp amplifier (GeneClamp 500; Axon Instruments) interfaced with a 16-bit AD/DA converter (Digidata 1200A; Axon Instruments). Electrodes filled with 140 mM KCl had an electric resistance of 0.5–1 MΩ. Voltage pulses were delivered every 15 s from a holding potential of −80 mV. Current records were sampled at 10 kHz and low pass-filtered at 2 kHz using an eight-pole Bessel filter and stored on computer for subsequent analysis. The extracellular recording solution contained (in mM): 88 NaCl, 10 KCl, 2 $MgCl_2$, 0.5 $CaCl_2$, 0.5 niflumic acid, 5 HEPES, 0.1% bovine serum albumin, pH 7.4 (NaOH). Leak and capacitive currents were subtracted on-line by a P/4 protocol. Residual capacitive artifacts were blanked for display purposes. Toxin solutions were superfused in the recording chamber at a flow rate of 2 ml/min using a ValveBank4 apparatus (Automate Scientific Inc.). The results are presented as mean ± S.D.

RESULTS AND DISCUSSION

Solid-phase Synthesis and Physicochemical Characterization of MTX_{Tyr} and MTX_{Pi1}—Stepwise assembly of MTX_{Tyr} was achieved by means of Fmoc/*t*-butyl chemistry (19). For Tyr^{32}, we used the more acid-resistant, but TFMSA-sensitive, 2,6 dichloro-benzyl side-chain protecting group that is not cleaved by trifluoroacetic acid treatment. A double coupling strategy was applied with Fmoc-amino acid hydroxybenzotriazole active esters. The yield of assembly ranged between 80 and 90%. Fig. 2 illustrates the elution profiles by C_{18} reversed-phase HPLC of MTX_{Tyr} and MTX_{Pi1} at different steps of the synthesis: crude reduced MTX_{Tyr} after trifluoroacetic treatment (*A*), crude oxidized MTX_{Tyr} after oxidative folding (*B*), MTX_{Pi1} resulting from TFMSA treatment of MTX_{Tyr} (*C*), and purified MTX_{Pi1} (*D*). These data suggest that the chemical strategy elaborated to synthesize MTX_{Pi1} appears to be successful. However, a careful physicochemical characterization was required, especially to formally establish that MTX_{Pi1} exhibits the expected Pi1-like disulfide bridging.

First the relative molecular mass of purified MTX_{Pi1} was verified by matrix-assisted laser desorption ionization-time of flight mass spectrometry analysis (Fig. 3*A*). An experimental M_r $(M+H)^+$ value of 3613.1 was obtained for MTX_{Pi1}, in close agreement with its deduced M_r $(M+H)^+$ of 3613.3. As expected, this experimental value also agrees with the experimental M_r $(M+H)^+$ of 3613.3 obtained for MTX (29). According to amino acid analysis after acidolysis of MTX_{Pi1}, the amino acid ratios were similar to the deduced values (Fig. 3*B*). The primary structure of MTX_{Pi1} was further verified by Edman sequencing (data not shown). To establish the half-cystine pairings of MTX_{Pi1}, the folded/oxidized peptide was treated with a mixture of trypsin and chymotrypsin. As shown in Fig. 3*C*, the data demonstrate that, contrary to MTX, MTX_{Pi1} exhibits half-cystine pairings between Cys^3-Cys^{24}, Cys^9-Cys^{29}, Cys^{13}-Cys^{31}, and Cys^{19}-Cys^{34} (which corresponds to the standard C1-C5, C2-C6, C3-C7, and C4-C8 Pi1-like pairings). Thus, as expected, MTX_{Pi1} differs from MTX by the two last disulfide bridges

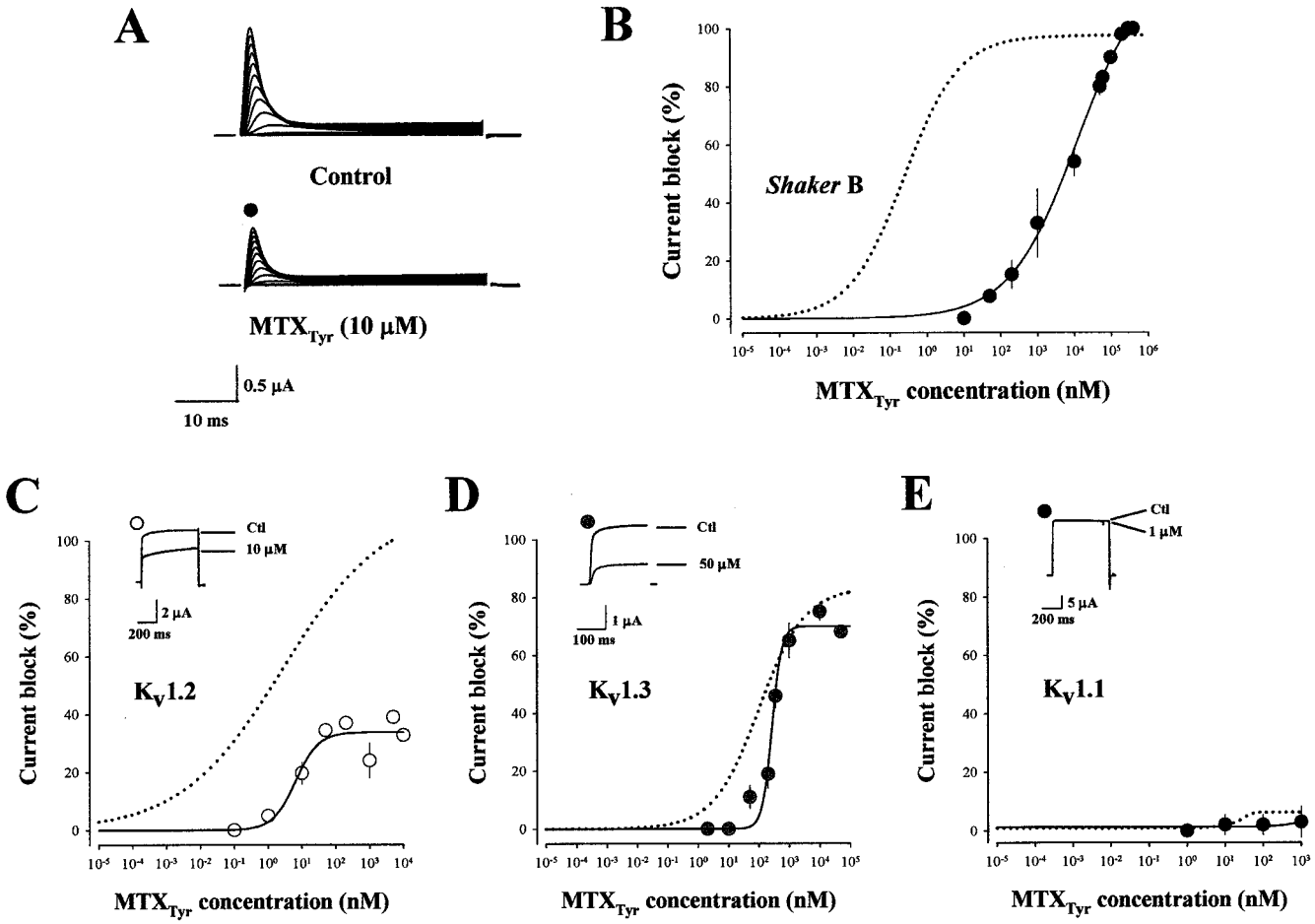

FIG. 7. **Chemical modification of Tyr^{32} alters MTX pharmacology.** *A*, current traces illustrating two sets of *Shaker* B K^+ currents elicited by various membrane depolarizations (from −40 to +70 mV) before and after application of 10 μM MTX_{Tyr}. Holding potential is −80 mV. *B*, dose-dependent inhibition curve of *Shaker* B currents by MTX_{Tyr}. Fitting parameters provide an IC_{50} value of 1229 ± 41 nM (n = 70), and a = 100 ± 7%. For comparison, the *dotted line* represents the dose-dependent inhibition curve by MTX_{Pi1}. Test potentials are +60 mV. *C*, dose-dependent inhibition curve of K_V1.2 currents by MTX_{Tyr}. IC_{50} = 6.5 ± 3.6 nM (n = 56), and a = 33.9 ± 2.7%. *Dotted line*, the effect of MTX_{Pi1}. *D*, dose-dependent inhibition curve of K_V1.3 currents by MTX_{Tyr}. IC_{50} = 287 ± 4 nM (n = 56), and a = 71.6 ± 3.5%. *Dotted line*, the effect of MTX_{Pi1}. *E*, no significant inhibition was observed on rat K_V1.1 for MTX_{Tyr} concentrations up to 1 μM (n = 28). Data points are the mean ± S.D. When absent, *error bars* are within symbol size.

(C3-C7 and C4-C8, instead of C3-C4 and C7-C8) and adopts a conventional pattern of disulfide bridging that is identical to those of other characterized α-KTx6 toxins (Fig. 3*D*).

Structural Properties of MTX_{Pi1}—The CD spectrum of MTX_{Pi1} was recorded to assess its secondary structures and was compared with the CD spectra of MTX and Pi1 (Fig. 4*A*). Measurements were performed at a wavelength ranging from 185–260 nm. The data obtained correspond essentially to π-π* and n-π* transitions of the amide chromophores of the peptide backbones (30). The CD spectra show large negative contributions between 207 and 230 nm and large positive contributions around 190 nm, indicating the presence of both α-helical and β-sheet structures. These data are consistent with peptide backbone folding according to α/β scaffolds (12) for MTX, MTX_{Pi1}, and Pi1. However, the CD spectra analyses do not point to obvious structural changes between MTX_{Pi1} and MTX. For the sake of comparison with the three-dimensional structure of MTX (11), we therefore generated a computed molecular model of MTX_{Pi1}. This model was obtained using MTX as a template; it was relaxed, minimized, and validated as described under "Experimental Procedures." As shown in Fig. 4*B*, the Cα backbone of MTX_{Pi1} does not differ markedly from that of MTX despite the important differences in half-cystine pairings. In contrast, a detailed examination of the side chains of a number of trifunctional amino acid residues suggests some marked differences in their orientations (Fig. 4*C*). These structural changes may nevertheless be sufficient to significantly impact peptide pharmacology.

Pharmacology of MTX_{Pi1}—MTX_{Pi1} was tested *in vivo* for neurotoxicity by intracerebroventricular injections in C57/BL6 mice. It is lethal in mice, with an LD_{50} value of 90 ng/mouse. In comparison, the LD_{50} values of MTX (2) and Pi1 (31) are 80 and 200 ng per mouse, respectively. MTX_{Pi1} remains as fully active as MTX *in vivo*, indicating that both disulfide bridge patterns provide peptides of equipotent lethality. Interestingly, oxidized MTX_{Tyr}, the intermediate reaction product that generates MTX_{Pi1} upon TFMSA treatment, is ~9-fold less potent than MTX_{Pi1} for lethal activity in mice, with an LD_{50} value of 800 ng/mouse. This result suggests that the integrity of Tyr^{32} is key to expression of MTX_{Pi1} lethality.

To investigate the pharmacology of MTX_{Pi1}, we first tested its ability to compete with ^{125}I-apamin for binding onto SK channels of rat brain synaptosomes (Fig. 5). MTX_{Pi1} inhibits ^{125}I-apamin binding with an IC_{50} value of 17.4 ± 5.6 nM. It is about 4-fold less potent than MTX, which exhibits an IC_{50} value of 4.4 ± 3.1 nM, in agreement with previous data (2). Therefore, the disulfide bridge pattern of the peptide (MTX-type *versus* Pi1-type) appears to mildly affect its binding onto rat brain apamin-sensitive SK channels. Additionally, the presence of the 2,6 dichloro-benzyl protecting group on Tyr^{32} sig-

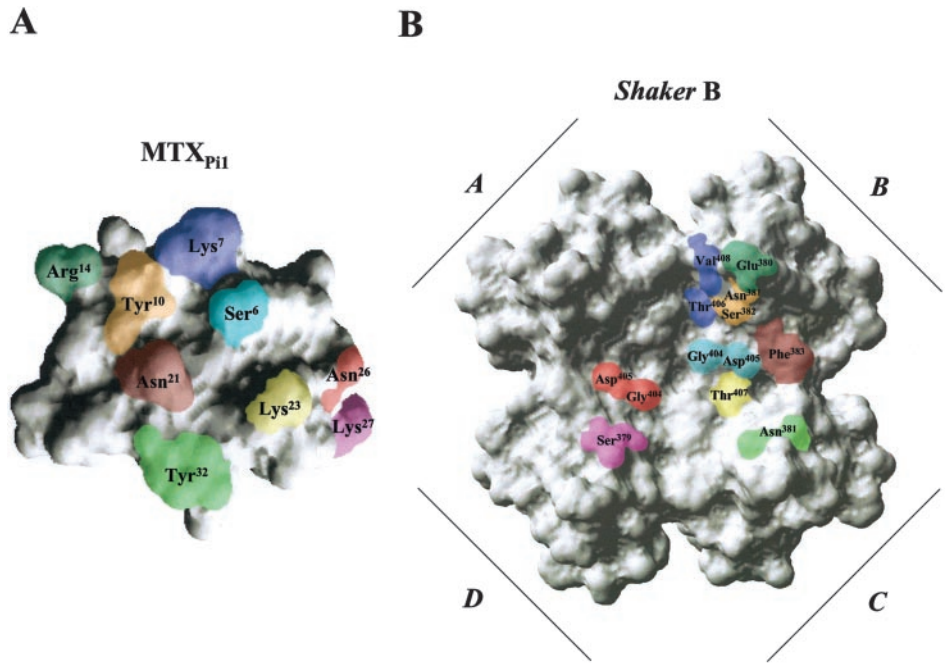

FIG. 8. **Map detailing major molecular contacts between MTX_{Pi1} and *Shaker* B channel.** *A*, space-filling representation of the molecular model of MTX_{Pi1}. *B*, space-filling representation of the molecular model of *Shaker* B channel (S5-H5-S6 pore regions). The pore regions of each four α-subunits composing the ion channel are labeled *A*, *B*, *C*, and *D*. Identical *color codes* were used to highlight pairs of interacting amino acid residues in *panels A* and *B*. *Numbers* represent the positions of the specified amino acid residues within either MTX_{Pi1} (*A*) or *Shaker* B channel (*B*) primary structure. The docking of MTX_{Pi1} onto the *Shaker* B channel can be imagined by a 180 ° vertical rotation of MTX_{Pi1} from left to right. Note that the *scale of magnification* between *panels A* and *B* is different.

nificantly decreased the ability of the peptide to compete with ^{125}I-apamin for binding to SK channel (IC_{50} value of 2.6 ± 0.3 μM; 150-fold less potent).

Next, we tested the effects of MTX_{Pi1} and MTX_{Tyr} onto *Shaker* B, rat $K_v1.1$, $K_v1.2$, and $K_v1.3$ expressed in *Xenopus* oocytes, because they are the regular targets of MTX (1, 2). As shown in Fig. 6*A*, MTX_{Pi1} blocks *Shaker* B K^+ outward currents with high affinity. The peptide starts to be active at 10 pM concentration and achieves the highest current block (97.7%) at about 10 nM. The effect of 10 nM MTX_{Pi1} is readily reversible upon washout of the peptide (Fig. 6*B*). The effect of MTX_{Pi1} is concentration-dependent with an IC_{50} value of current inhibition of 0.24 ± 0.12 nM (n = 63; Fig. 6*C*). This should be compared with the effect of MTX, which acts on *Shaker* B channels with an IC_{50} of 3.4 nM (9) in identical experimental conditions. These data indicate that the MTX peptide is ~14-fold more potent in binding onto *Shaker* B channels when reticulated with Pi1-like half-cystine pairings rather than with its wild-type pairings. For rat $K_v1.2$ channels, the extent of K^+ current blockage by MTX_{Pi1} is maximal with an IC_{50} value of 2.8 ± 2.1 nM. Compared with MTX, these values correspond to a 46-fold reduction in affinity but to an increase of about 30% in the extent of blockage (16). Altogether, the data obtained for *Shaker* B and $K_v1.2$ channels suggest that the change in disulfide bridging of the MTX peptide is accompanied, not only by modifications in affinity, but also by changes in the combined efficacy of ionic pore occlusion and K^+ efflux by the peptide. This analysis is reinforced by examining the effect of MTX_{Pi1} on rat $K_v1.3$ K^+ currents (Fig. 6*E*). MTX_{Pi1} interacts with $K_v1.3$ channels with an IC_{50} value of 102 ± 37 nM (n = 63), which represents a 3-fold increase in affinity as compared with MTX (16). Interestingly, MTX_{Pi1} also blocks the K^+ efflux to a greater extent (83 ± 4%) than MTX (~20%). A similar change in blocking efficacy toward $K_v1.3$ channel had already been observed with a three-disulfide-bridged MTX analog (16), suggesting that the peptide half-cystine pairing pattern may significantly affect ion channel pore occlusion. Finally, we also investigated the effect of MTX_{Pi1} on rat $K_v1.1$ K^+ currents (Fig. 6*F*) and found it to be mostly inactive, as reported for MTX (16).

To get some insight on the contribution of Tyr^{32} residue to MTX_{Pi1} pharmacology, we also investigated the effects of folded/oxidized MTX_{Tyr} on the various voltage-gated K^+ channels (Fig. 7). Interesting marked differences in the pharmacological properties of this peptide were observed, as compared with those of MTX_{Pi1}. Tyr^{32} appears to be key with regard to MTX_{Pi1} affinity for *Shaker* B channel but not for the extent of K^+ current blockage (Fig. 7, *A* and *B*). Indeed, with an IC_{50} value of 1,229 ± 41 nM (n = 70), the folded/oxidized MTX_{Tyr} is about 5,000-fold less potent than MTX_{Pi1} for K^+ channel interaction. For rat $K_v1.2$ channels, an inverted situation is observed (Fig. 7*C*). The IC_{50} value obtained for MTX_{Tyr} is grossly similar to that of MTX_{Pi1} (6.5 ± 3.6 nM and 2.8 ± 2.1 nM, respectively), contrary to the extent of current blockage, which is markedly decreased from 100% to 34 ± 3% in the case of MTX_{Tyr}. These findings further support a key role of MTX Tyr^{32} residue for toxin effect on $K_v1.2$ channel, as reported previously (8). In contrast, the presence of a 2,6 dichloro-benzyl moiety on the Tyr^{32} phenol ring has no significant impact on rat $K_v1.3$ (Fig. 7*D*) or $K_v1.1$ (Fig. 7*E*) K^+ channel pharmacology.

Docking of MTX_{Pi1} onto Voltage-gated K^+ Channels—We first performed a Blastp (V.2.2.5, us.expasy.org/tools/blast/) search against the whole Protein Data Bank to select the correct template to generate models of the S5-H5-S6 portions of rat $K_v1.1$, $K_v1.2$, $K_v1.3$, and *Shaker* B channels. The KcsA primary structure (Swiss-Prot number 1BL8) showed the best *E*-value score for all the voltage-gated K^+ channels under consideration. In addition, CLUSTALW (V.1.82) amino acid sequence alignments indicate that KcsA channel is a premium template that presents sequence homologies of 69.8% ($K_v1.1$), 70.1% ($K_v1.2$), 69.1% ($K_v1.3$), and 65.6% (*Shaker* B). The three-dimensional structures of the molecular models generated were very similar to that of KcsA, with root mean square deviation values of 0.48 Å ($K_v1.1$), 1.93 Å ($K_v1.2$), 0.32 Å ($K_v1.3$), and 1.68 Å (*Shaker* B). The geometric quality of the models was assessed

by the PROCHECK software (V.3.5.4). No amino acid residue was found to be in disallowed regions, thereby validating the structural properties of the models (data not shown). The three-dimensional structure of MTX (11) and the molecular models of both MTX_{Pi1} and Pi1 were used in docking experiments with the different models of voltage-gated K^+ channels. Docking energies were calculated according to the procedures described under "Experimental Procedures."

We first detailed the docking of MTX_{Pi1} on *Shaker* B channel as it exerts its highest affinity toward this K^+ channel subtype (IC_{50} value of 0.24 nM). Fig. 8 illustrates the amino acid residues of MTX_{Pi1} (Fig. 8*A*) that may interact with *Shaker* B channel residues (Fig. 8*B*), as identified according to docking simulation. It is worth noting that the Lys^{23} and Tyr^{32} residues of MTX_{Pi1} belong to the functional dyad that is reported to be crucial for toxin bioactivity (8, 9, 32).

Docking simulations suggest that MTX_{Pi1} and MTX possess similar overall interaction topologies. For example, the Lys^7 and Lys^{23} residues share the same interacting residues on *Shaker* B channel (the pair Thr^{406} and Val^{408} for Lys^7, and Thr^{407} for Lys^{23}; data not shown for MTX). Interestingly, additional analyses show that MTX_{Pi1} possess specific molecular contacts (Asn^{26} with Gly^{404} and Asp^{405}) that are not observed in the MTX docking simulations. Moreover, MTX_{Pi1} seems to be more stabilized than MTX on *Shaker* B channel because of a greater number of molecular contacts with the outer loop domain (Glu^{380}, Asn^{381}, and Ser^{382}). One should note that Lys^{27} of MTX_{Pi1} also interacts with Ser^{379} of *Shaker* B channel, whereas Lys^{27} of MTX does not interact with any ion channel amino acid residue. This may reasonably explain the 14-fold difference in IC_{50} values observed experimentally for MTX_{Pi1} and MTX. Next, we correlated the docking energies of MTX_{Pi1}, MTX, and Pi1 on *Shaker* B channel with their experimentally observed IC_{50} values (Fig. 9*A*). A high degree of correlation ($r^2 = 0.97$) was observed between docking energies and IC_{50} values, which validates our overall molecular modeling approach. It also indicates that more detailed investigations of the interaction between MTX_{Pi1} and *Shaker* B channel will be permitted.

On $K_v1.1$ channel, MTX_{Pi1}, MTX, and Pi1 are not significantly active. In agreement with these data, no satisfying docking solutions were obtained for these peptides. Thus, we next investigated the docking properties of the peptides on $K_v1.2$ channel (Fig. 9*B*). MTX_{Pi1} ($IC_{50} = 2.8$ nM) is, respectively, 46- and 6-fold less active than MTX ($IC_{50} = 0.06$ nM) and Pi1 ($IC_{50} = 0.44$ nM) on $K_v1.2$. Docking simulations indicate that MTX_{Pi1}, MTX, and Pi1 share basically a common interaction map with $K_v1.2$, although some subtle differences could be observed that may explain their distinct affinities. The Thr^4, Lys^7, and Asp^8 residues of both MTX and MTX_{Pi1} are in contact with identical amino acid residues, Gly^{378} and Asp^{379}, of the $K_v1.2$ ion channel pore (data not shown). The major difference concerns Lys^{27}, which stabilizes MTX over the pore surface by interacting with Ser^{356}. A previous study has also shown that Lys^{27} of MTX (as well as Lys^{23} and Lys^{30}) is crucial for $K_v1.2$ recognition (33). In contrast, according to our docking experiments, Lys^{27} of MTX_{Pi1} does not interact with any $K_v1.2$ amino acid residue. This difference in Lys^{27} behavior for its interaction with $K_v1.2$ may thus explain the 46-fold decrease in $K_v1.2$ affinity of MTX_{Pi1} over MTX. Similar docking experiments were performed for Pi1 (data not shown). As for *Shaker* B channel, the docking experiments on $K_v1.2$ channel indicate a very good correlation ($r^2 = 0.99$) between the docking energies of MTX_{Pi1}, MTX, and Pi1, and the experimental IC_{50} values thereof (Fig. 9*B*).

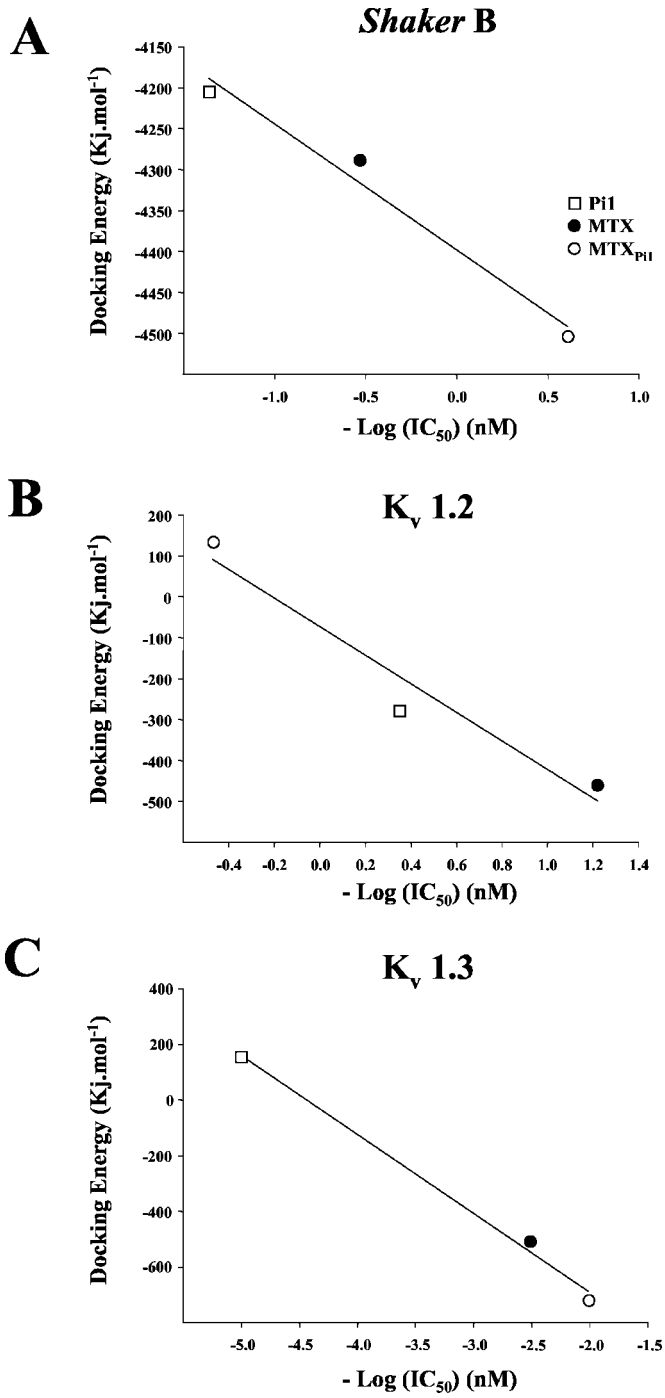

FIG. 9. **Linear regressions showing the correlation between docking energies and experimental IC_{50} values.** *A*, docking of MTX_{Pi1}, MTX, and Pi1 onto *Shaker* B channel. *B*, same as in *panel A*, but rat $K_v1.2$ channel. *C*, same as in *panel A*, but rat $K_v1.3$ channel. For this ion channel subtype, we considered an IC_{50} value of 100 μM for Pi1 (31).

Docking simulations performed with the three peptides on rat $K_v1.3$ channel correlate well with the actual peptide pharmacologies. Relatively low-scoring interactions between MTX_{Pi1} and $K_v1.3$ channel or MTX and $K_v1.3$ channel were found (data not shown), consistent with their experimental IC_{50} values. In addition, computed data on Pi1 docking show the existence of very few contacts between Pi1 and the $K_v1.3$ channel. As for other docking simulations, a high degree of linear correlation ($r^2 = 0.99$) was also obtained between the experimental IC_{50} values and the docking energies of these peptides (Fig. 9*C*).

In this study, we generated molecular models of the various voltage-gated K^+ channels using the KcsA structure as template. The structure of a novel K^+ channel (KvAP) from *Aeropyrum pernix* has recently been described, after our own structural analyses were completed (34). Of note, this K^+ channel is voltage-dependent, contrary to the KcsA channel. However, a careful comparison of the pore regions (S_5-H_5-S_6 segments) of KvAP and KcsA reveals an almost perfect superimposition of the α-carbon traces of both channels. In addition, the selectivity filter is essentially identical to that of KcsA. Despite these marked structural similarities, we also generated molecular models of the *Shaker* B, $K_v1.2$, and $K_v1.3$ channels using the KvAP channel as template instead of KcsA. In each case, models generated using either KcsA or KvAP as template were identical (data not shown), thereby validating the use of KcsA as template in our study.

Concluding Remarks—In the present work, we show that, by using a particular strategy of solid-phase peptide synthesis, one can act on the final half-cystine pairing pattern of a reticulated peptide without altering its chemical structure by either mutations or chemical modifications of specific amino acid residues, or both. Docking experiments ease the understanding of the molecular basis of the toxin to ion channel recognition. In the case of voltage-gated K^+ channels, it was generally well admitted that this recognition was solely based on the participation of amino acid residues from the toxin β-sheet structure. This does not appear to be the case because docking data suggest the contribution of amino acid residues belonging to distinct toxin structural domains (*e.g.* Ser^6, Lys^7, and Tyr^{10} of MTX). From this study, the disulfide bridge organization of MTX contributes to its pharmacological action. Though the α/β scaffold is neither disrupted nor markedly altered, we highlighted some interesting differences in the relative orientation of the side chains of certain "key" amino acid residues. Therefore, it is likely that the most significant changes in pharmacological properties observed between MTX_{Pi1} and MTX may be in part attributed to the side chains of Arg^{14}, Lys^{27}, and/or Tyr^{32} residues. In line with such a view, a recent study (33) based on Brownian dynamics simulations argues in favor of central roles played by Lys^{27} and Tyr^{32} residues of MTX in its recognition of the Kv1.2 channel.

Acknowledgments—We thank P. Mansuelle, B. Chagot, J. Barbaria, C. Devaux, J. Van Rietschoten, and B. De Rougé for help in this work.

REFERENCES

1. Kharrat, R., Mansuelle, P., Sampieri, F., Crest, M., Oughideni, R., Van Rietschoten, J., Martin-Eauclaire, M. F., Rochat, H., and El Ayeb, M. (1997) *FEBS Lett.* **406,** 284–290
2. Kharrat, R., Mabrouk, K., Crest, M., Darbon, H., Oughideni, R., Martin-Eauclaire, M. F., Jacquet, G., El Ayeb, M., Van Rietschoten, J., and Sabatier, J. M. (1996) *Eur. J. Biochem.* **242,** 491–498
3. Olamendi-Portugal, T., Gomez-Lagunas, F., Gurrola, G. B., and Possani, L. (1996) *Biochem. J.* **315,** 977–981
4. Olamendi-Portugal, T., Gomez-Lagunas, F., Gurrola, G. B., and Possani, L. D. (1998) *Toxicon* **36,** 759–770
5. Lebrun, B., Romi-Lebrun, R., Martin-Eauclaire, M. F., Yasuda, A., Ishiguro, M., Oyama, Y., Pongs, O., and Nakajima, T. (1997) *Biochem. J.* **328,** 321–327
6. Savarin, P., Romi-Lebrun, R., Zin-Justin, S., Lebrun, B., Nakajima, T., Gilquin, B., and Ménez, A. (1999) *Protein Sci.* **8,** 2672–2685
7. Tytgat, J., Chandy, G., Garcia, M. L., Gutman, G. A., Martin-Eauclaire, M-F., van der Walt, J. J., and Possani, L. D. (1999) *Trends Pharmacol. Sci.* **20,** 444–447
8. Castle, N. A., London, D. O., Creech, C., Fajloun, Z., Stocker, J. W., and Sabatier, J. M. (2003) *Mol. Pharmacol.* **63,** 409–418
9. Carlier, E., Avdonin, V., Geib, S., Fajloun, Z., Kharrat, R., Rochat, H., Sabatier, J. M., Hoshi, T., and De Waard, M. (2000) *J. Peptide Res.* **55,** 419–427
10. Avdonin, V., Nolan, B., Sabatier, J. M., De Waard, M., and Hoshi, T. (2000) *Biophys. J.* **79,** 776–787
11. Blanc, E., Sabatier, J. M., Kharrat, R., Meunier, S., El Ayeb, M., Van Rietschoten, J., and Darbon, H. (1997) *Proteins* **29,** 321–333
12. Bontems, F., Roumestand, C., Gilquin, B., Ménez, A., and Toma, F. (1991) *Science* **254,** 1521–1523
13. Mosbah, A., Kharrat, R., Fajloun, Z., Renisio, J. G., Blanc, E., Sabatier, J. M., El Ayeb, M., and Darbon, H. (2000) *Proteins* **40,** 436–442
14. Delepierre, M., Prochnicka-Chalufour, A., and Possani, L. D. (1997) *Biochemistry* **36,** 2649–2658
15. Delepierre, M., Prochnicka-Chalufour, A., and Possani, L. D. (1998) *Toxicon* **36,** 1599–1608
16. Fajloun, Z., Ferrat, G., Carlier, E., Fathallah, M., Lecomte, C., Sandoz, G., di Luccio, E., Mabrouk, K., Legros, C., Darbon, H., Rochat, H., Sabatier, J. M., and De Waard, M. (2000) *J. Biol. Chem.* **275,** 13605–13612
17. Carlier, E., Fajloun, Z., Mansuelle, P., Fathallah, M., Mosbah, A., Oughideni, R., Sandoz, G., Di Luccio, E., Geib, S., Regaya, I., Brocard, J., Rochat, H., Darbon, H., Devaux, C., Sabatier, J. M., and De Waard, M. (2001) *FEBS Lett.* **489,** 202–207
18. Fajloun, Z., Mosbah, H., Carlier, E., Mansuelle, P., Sandoz, G., Fathallah, M., di Luccio, E., Devaux, C., Rochat, H., Darbon, H., De Waard, M., and Sabatier, J. M. (2000) *J. Biol. Chem.* **275,** 39394–39402
19. Merrifield, R. B. (1986) *Science* **232,** 341–347
20. Tam, J. P., Heath, W. F., and Merrifield, R. B. (1986) *J. Am. Chem. Soc.* **108,** 5242–5251
21. Laskowski, R. A., MacArthur, M. W., Moss, D. S., and Thornton, J. M. (1993) *J. Appl. Cryst.* **26,** 283–291
22. Morris, A. L., MacArthur, M. W., Hutchinson, E. G., and Thornton, J. M. (1992) *Proteins* **12,** 345–364
23. Palma, P. N., Krippahl, L., Wampler, J. E., and Moura, J. J. (2000) *Proteins* **39,** 372–384
24. Nicholls, A., Sharp, K. A., and Honig, B. (1991) *Proteins* **11,** 281–296
25. Stocker, U., and van Gunsteren, W. F. (2000) *Proteins* **40,** 145–153
26. Wallace, A. C., Laskowski, R. A., and Thornton, J. M. (1995) *Protein Eng.* **8,** 127–134
27. Gray, E. G., and Whittaker, V. P. (1962) *J. Anat.* **96,** 79–88
28. Eppig, J. J., and Dumont, J. N. (1976) *In Vitro* **12,** 418–427
29. di Luccio, E., Azulay, D. O., Regaya, I., Fajloun, Z., Sandoz, G., Mansuelle, P., Kharrat, R., Fathallah, M., Carrega, L., Estève, E., Rochat, H., De Waard, M., and Sabatier, J. M. (2001) *Biochem. J.* **358,** 681–692
30. Jonhson, W. C., Jr. (1985) *Methods Biochem. Anal.* **31,** 61–163
31. Fajloun, Z., Carlier, E., Lecomte, C., Geib, S., di Luccio, C., Bichet, D., Mabrouk, K., Rochat, H., De Waard, M., and Sabatier, J. M. (2000) *Eur. J. Biochem.* **267,** 5149–5155
32. Darbon, H., Blanc, E., and Sabatier, J. M. (1999) in *Perspectives in Drug Discovery and Design*: *Animal Toxins and Potassium Channels* (Darbon, H., and Sabatier, J. M., eds) Vols. 15/16, pp. 41–60, Kluwer Academic Publishers, Dordrecht, The Netherlands
33. Fu, W., Cui, M., Briggs, J. M., Huang, X., Xiong, B., Zhang, Y., Luo, X., Shen, J., Ji, R., Jiang, H., and Chen, K. (2002) *Biophys. J.* **83,** 2370–2385
34. Jiang, Y., Lee, A., Chen, J., Ruta, V., Cadene, M., Chait, B. T., and MacKinnon, R. (2003) *Nature* **423,** 33–41

A Maurotoxin with Constrained Standard Disulfide Bridging: INNOVATIVE STRATEGY OF CHEMICAL SYNTHESIS, PHARMACOLOGY, AND DOCKING ON K+ CHANNELS

Sarrah M'Barek, Ignacio Lopez-Gonzalez, Nicolas Andreotti, Eric di Luccio, Violeta Visan, Stephan Grissmer, Susan Judge, Mohamed El Ayeb, Hervé Darbon, Hervé Rochat, François Sampieri, Evelyne Béraud, Ziad Fajloun, Michel De Waard and Jean-Marc Sabatier

J. Biol. Chem. 2003, 278:31095-31104.
doi: 10.1074/jbc.M304271200 originally published online June 3, 2003
